

Jet from Binary Neutron Star Merger with Prompt Black Hole Formation

Kota Hayashi^{1,2}, Kenta Kiuchi^{1,2}, Koutarou Kyutoku^{1,3,4}, Yuichiro Sekiguchi⁵, and Masaru Shibata^{1,2}

¹Max Planck Institute for Gravitational Physics (Albert Einstein Institute), Am Mühlenberg 1, Postdam-Golm 14476, Germany

²Center for Gravitational Physics and Quantum Information, Yukawa Institute for Theoretical Physics,
Kyoto University, Kyoto 606-8502, Japan

³Department of Physics, Graduate School of Science, Chiba University, Chiba 263-8522, Japan

⁴Interdisciplinary Theoretical and Mathematical Sciences Program (iTHEMS), RIKEN, Wako, Saitama 351-0198, Japan

⁵Department of Physics, Toho University, Funabashi, Chiba 274-8510, Japan



(Received 14 October 2024; revised 17 February 2025; accepted 9 April 2025; published 30 May 2025)

We performed the longest numerical-relativity neutrino-radiation magnetohydrodynamics simulation for a binary neutron star merger that extends to ≈ 1.5 s after the merger. We consider the binary model that undergoes the prompt collapse to a black hole after the merger with asymmetric mass $1.25M_{\odot}$ and $1.65M_{\odot}$ and SFHo equation of state. We find the Poynting flux-driven collimated outflow as well as the gravitational wave emission, neutrino emission, dynamical mass ejection, and postmerger mass ejection facilitated by magnetorotational instability-driven turbulent viscosity in a single self-consistent binary neutron star merger simulation. A magnetosphere dominated by the aligned global magnetic field penetrating the black hole develops along the black-hole spin axis after the turbulence in the remnant disk is enhanced. A jet with the Poynting flux with isotropic-equivalent luminosity of $\sim 10^{49}$ erg/s is launched, and the duration of the high luminosity is expected to be $O(1)$ s.

DOI: 10.1103/PhysRevLett.134.211407

Introduction—Multimessenger astrophysics, including gravitational wave (GW) detection, began with the observation of GW170817, AT2017gfo, and GRB170817A from a binary neutron star (BNS) merger [1–6]. The GWs constrain the nuclear equation of the state (EOS) of neutron star (NS) matter [1,7–10]. The kilonova emission indicated that neutron-rich matter is likely ejected from the system [11–14], with the synthesis of heavy elements by the *r* process (rapid neutron capture process) [15–20]. The detection of a short-hard γ -ray burst (SGRB) indicated that the relativistic jet was launched from the system [12,21,22].

Two years later, GW190425 revealed that the binary system with large total mass $\sim 3.4M_{\odot}$ exists [23]. The GW signal is consistent with BNS merger [though the heavy component of the system being a black hole (BH) is not ruled out [24,25]]. The total mass of the system is larger than the BNS systems known [26,27] and it is expected to experience a prompt collapse to the BH after the merger [28–35]. Since this event was a single detector event, the sky localization was poor, and an electromagnetic counterpart associated with this event was not detected [36].

However, if the mass asymmetry is large, we may expect that the system undergoes the prompt collapse to a BH with a massive disk remaining [29,37]. If the GW event from such a source is detected with sufficient localization, the associated electromagnetic counterparts could be expected, as was the case for GW170817.

The theoretical modeling of the entire evolution for the prompt-collapse BNS merger and the prediction of the multimessenger signals are highly demanded to interpret the foreseen observation. For this purpose, it is crucial to perform numerical relativity simulations incorporating magnetohydrodynamics and neutrino-radiation transfer. Further, the simulation has to cover an entire evolution stage extending $O(1)$ s for the postmerger stage in order to self-consistently explore the mass ejection and jet launch.

Since 2005, BNS merger simulations with magnetohydrodynamics and/or microphysics of the NS matter focusing on the merger and early postmerger stage have been performed [38–69]. Also, simulations for BNS merger remnants, focusing on the postmerger stage, have been recently done [70–87]. However, these simulations have limitations in that they were not long enough to explore the entire postmerger evolution, or they employed non-self-consistent initial data. Only Ref. [88] has successfully simulated the entire evolution of BNS merger self-consistently. Concerning the prompt-collapse BNS case, Ref. [56] has performed general relativistic magnetohydrodynamics simulations. It showed that up to ~ 26 ms after the merger, there is no evidence for aligned magnetic-field

Published by the American Physical Society under the terms of the [Creative Commons Attribution 4.0 International license](#). Further distribution of this work must maintain attribution to the author(s) and the published article's title, journal citation, and DOI. Open access publication funded by the Max Planck Society.

formation in the polar region and Poynting flux-driven outflow. However, this timescale may not be long enough to explore the jet launch since the event GW170817 and GRB170817A had a time lag of ≈ 1.7 s [1–3] and black hole–neutron star (BHNS) merger simulations showed that it requires 200 ms $\lesssim t \lesssim 3$ s after the merger for magnetosphere formation and Poynting flux launching depending on the binary models [89,90].

In order to delineate the entire picture of the prompt-collapse BNS merger, we performed a second-long numerical-relativity neutrino-radiation magnetohydrodynamics simulation on the Japanese supercomputer Fugaku. This Letter reports the multimessenger signals driven by the prompt-collapse BNS merger focusing especially on the launch of the Poynting flux-driven collimated outflow, i.e., jet.

Numerical methods and model—The numerical method used in this work is the same as that summarized in Ref. [48]. We solve Einstein’s equation by a puncture-Baumgarte-Shapiro-Shibata-Nakamura formalism [91–95] with the Z4c constraint propagation prescription [96–98]. The fourth-order finite differentiation in space and time discretizes the equation. The magnetohydrodynamics equations are solved using the HLLD Reimann solver [99] with the constrained transport scheme [100] and the divergence-free- and magnetic-flux-preserving mesh refinement scheme [101,102]. Our code implements the gray M1 + Leakage scheme for the neutrino radiation transfer to take into account the neutrino cooling and heating [77,86,103–105].

The NS matter is modeled by nuclear-theory-based finite-temperature EOS, SFHo [106], for a high-density range and Helmholtz EOS [107] for a low-density range. The maximum mass of the isolated nonrotating NS with SFHo is $2.06M_{\odot}$. The LORENE library [108] is employed to prepare an asymmetric irrotational BNS with mass $M_1 = 1.25M_{\odot}$ and $M_2 = 1.65M_{\odot}$ in quasiequilibrium, assuming the neutrinoless β -equilibrium cold state, as the initial data. The initial orbital frequency Ω_0 is set to be $\Omega_0 m_0 G/c^3 = 0.025$, where $m_0 = M_1 + M_2$, c the speed of light, and G gravitational constant.

We initially superimposed a poloidal magnetic field confined inside the NS. The magnetic field is given in terms of the vector potential as

$$A_j = \{-(y - y_{\text{NS}})\delta_j^x + (x - x_{\text{NS}})\delta_j^y\} \times A_b \max(P/P_{\text{max}} - 2 \times 10^{-4}, 0)^{0.5}, \quad (1)$$

where x_{NS} and y_{NS} are the coordinate center of each NS, P and P_{max} are the pressure and its maximum value, respectively, and A_b is constant and set so that the maximum magnetic-field strength becomes 10^{15} G. This definition is similar to that which is in, e.g., Refs. [47,88], but differs for

the power index 0.5 instead of 2 used in the previous works. We intended both NSs to have a strong magnetic field that extends to their surface. Even for the realistic initial magnetic field, we expect the Kelvin-Helmholtz instability to be activated at the shear structure appearing at the contact interface of the spiral arm and amplify the magnetic field in a short timescale. With this, a strong magnetic field remains in the massive disk formed after the prompt BH formation. The strong initial magnetic field is essential to resolve magnetorotational instability (MRI) in the remnant disk with limited grid resolution.

This simulation is performed on a fixed-mesh refinement domain with 14 refinement levels. The grid resolution in the finest level is $\Delta x_{14} = 150$ m and the coarser domain has the resolution of $\Delta x_l = 2\Delta x_{l+1}$, where $l = 1, \dots, 13$. The finest domain covers $[-38.1 \text{ km}, 38.1 \text{ km}]^3$ and the whole computational domain is $[-312, 115.2 \text{ km}, 312, 115.2 \text{ km}]^3$ in the Cartesian coordinates.

We set the atmosphere with the rest-mass density 10^3 g/cm^3 for the finest domain and $10^3(r/38.1 \text{ km})^{-3} \text{ g/cm}^3$ for the coarser domains where r is the radial coordinate. We assume the constant density once the atmosphere density reaches $\approx 0.166 \text{ g/cm}^3$. We set the temperature and the electron fraction of the atmosphere to be 10^{-3} MeV and 0.5, respectively.

The computational cost is about 130×10^6 CPU hours. Each job was carried out using 20 736–82 944 CPUs on Fugaku.

Inspiral and merger—The BNS merger can be characterized by three stages: inspiral, merger, and postmerger stages. In the present simulation, the system inspirals for five orbits before the merger. In this stage, the magnetic field plays essentially no role since the ratio of the electromagnetic field energy to the internal energy is less than 10^{-6} . Since the total mass of the system is high $m_0 = 2.9M_{\odot}$ the merged NSs collapse promptly in the merger stage [28–30,32,109,110], forming a BH with its mass $\approx 2.77M_{\odot}$ and dimensionless spin ≈ 0.76 [111].

We define the merger time $t_{\text{merger}} = 16.4$ ms at which the amplitude of GWs becomes maximum. Since the binary is highly asymmetric, a massive disk is formed around the BH after the merger [29,37]. The baryonic mass of the disk at $t - t_{\text{merger}} \approx 20$ ms is $\approx 6.2 \times 10^{-2}M_{\odot}$.

Poynting flux-driven outflow—Figure 1 displays the 3D snapshot at $t - t_{\text{merger}} \approx 1.3$ s in a domain of $\sim 10^3$ km and $\sim 10^2$ km. The rest-mass density, magnetic-field lines penetrating the apparent horizon, and the outflow in the magnetically dominated region are shown. We find that along the BH spin axis, the magnetosphere is developed due to the large-scale magnetic field produced by the MRI-driven $\alpha\Omega$ dynamo [112–114]. In this magnetosphere, we find an outgoing Poynting flux with its isotropic-equivalent luminosity $\approx 10^{49}$ erg/s and its duration of $\sim O(1)$ s that

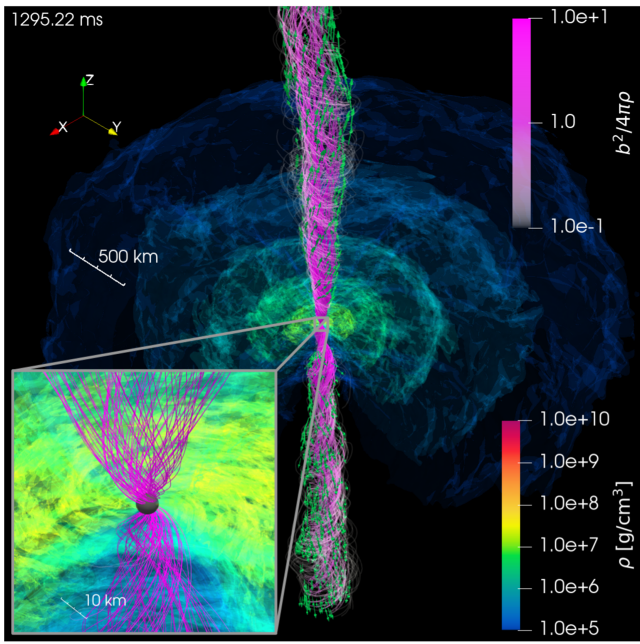


FIG. 1. The 3D snapshot at $t - t_{\text{merger}} \approx 1.3$ s in a domain of $\sim 10^3$ km and $\sim 10^2$ km. The rest-mass density (contours), magnetic-field lines penetrating the apparent horizon (lines), and the outflow in the magnetosphere (arrows) are shown. The black sphere at the center shows the apparent horizon. See also the animation [115] and interactive 3D snapshot [116].

could power an SGRB (see below for more details). The luminosity is lower than the typically observed SGRBs [21,22], but the duration is consistent. Below we describe the magnetosphere formation process in detail.

After the merger in the remnant disk, the magnetic field is amplified by the winding [117] and MRI [118,119]. The fastest growing mode of the MRI is sufficiently resolved for $\rho \lesssim 10^{10}$ g/cm³ and $t - t_{\text{merger}} \gtrsim 0.02$ s, and fully resolved for whole disk for $t - t_{\text{merger}} \gtrsim 0.1$ s (see Supplemental Material [120]). Figure 2 plots the azimuthally averaged toroidal magnetic field along the polar direction at $r \approx 50$ km. In addition, the animation [126] displays the azimuthally averaged rest-mass density, poloidal magnetic field, MRI quality factor, and the Shakura-Sunyaev parameter on the $r-\theta$ plane. They show that as the MRI is resolved, a magnetic field with the opposite polarity is periodically generated near the equatorial plane in the disk. The generated magnetic field ascends to the polar region and accumulates there. As the magnetic field with the opposite polarity propagates, they cancel out each other and dissipate away due to the reconnection. The period for the polarity flips at $r \approx 50$ km is $\approx 0.03 - 0.04$ s which agrees with the period derived by the $\alpha\Omega$ dynamo theory [112–114] ≈ 0.03 s. The detailed analysis of the $\alpha\Omega$ dynamo will be reported in a separate paper [127]. These facts show that the MRI-driven $\alpha\Omega$ dynamo is activated, and the large-scale magnetic field with a length scale comparable to the size of the disk is generated.

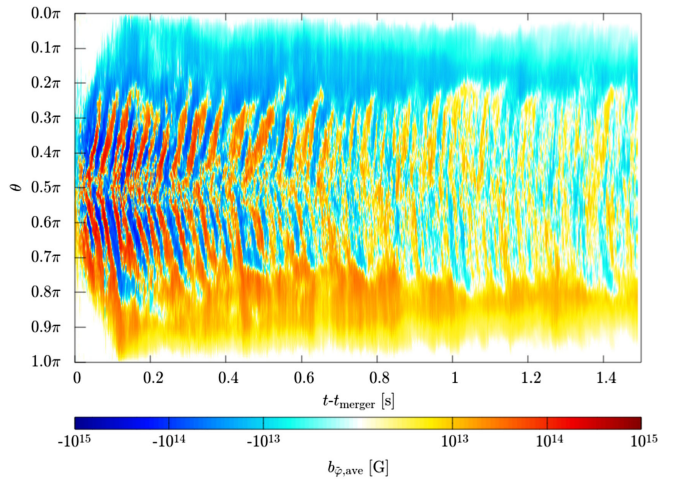


FIG. 2. The azimuthally averaged toroidal magnetic field along the polar direction at $r \approx 50$ km.

Once a part of the mean magnetic field in the polar region plunges into the BH, the BH spin can further amplify the toroidal magnetic field by the winding. This enhances the magnetic pressure at the polar region, and the magnetic field expands vertically to the disk. Along with this, the rest-mass density at this region decreases due to the accretion into the BH or expansion due to the aforementioned magnetic pressure. Eventually, a large-scale helical magnetic field around the spin axis is developed, and the magnetization parameter $b^2/4\pi\rho$ exceeds the unity forming a magnetosphere. Since this system undergoes the prompt collapse, the rest-mass density along the BH axis after the merger is lower than the nonprompt collapse case due to the lack of the fallback matter, and thus, it is easier to develop a magnetosphere compared to the nonprompt collapse case [88]. In this magnetically dominated region, the outgoing Poynting flux is launched and drives an outflow. By contrast, the Poynting flux-driven outflow was not launched until $t - t_{\text{merger}} \approx 1.1$ s in the nonprompt collapse case [88]. The magnetosphere developed is supported and collimated by the gas pressure from the matter.

Figure 3(a) plots the isotropic-equivalent Poynting luminosity evaluated on the sphere at $r \approx 500$ km and opening angle of 10° for the north and south hemispheres. It shows that the luminosity reaches $L_{\text{iso},500 \text{ km},10^\circ} \approx 10^{49}$ erg/s at $t - t_{\text{merger}} \approx 0.3$ s and 0.13 s for the north and south hemispheres, respectively. Since the magnetosphere is formed after at least ≈ 3 periods of the $\alpha\Omega$ dynamo cycle, it contributes to the launch of the Poynting flux. We found that this Poynting luminosity is powered by the Blandford-Znajek mechanism [128] by magnetic fields penetrating a rapidly spinning BH. Figure 3(a) also plots the Poynting luminosity $L_{500 \text{ km},10^\circ}$ confined in a region within $\theta < 10^\circ$ at $r \approx 500$ km and the Poynting luminosity $L_{\phi_{\text{AH},\text{local}}>10}$ evaluated at the region with $\phi_{\text{AH},\text{local}} > 10$ on the apparent horizon. Here, $\phi_{\text{AH},\text{local}}$ is the local MADness

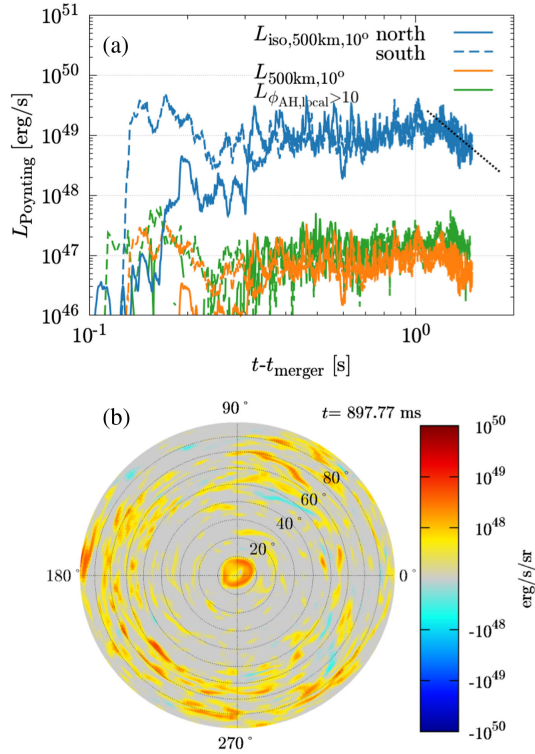


FIG. 3. The quantities related to the magnetically driven outflow. The top panel plots the Poynting luminosity $L_{500\text{ km},10^\circ}$ and isotropic-equivalent luminosity $L_{\text{iso},500\text{ km},10^\circ}$ evaluated at $r \approx 500$ km and opening angle with 10° . It also plots the Poynting luminosity $L_{\phi_{\text{AH},\text{local}} > 10}$ evaluated at the region with $\phi_{\text{AH},\text{local}} > 10$. The dotted line emphasizes the decreasing trend of the Poynting luminosity for $t - t_{\text{merger}} \gtrsim 1$ s. The bottom panel plots the angular distribution of the Poynting luminosity per steradian evaluated on the sphere at $r \approx 500$ km for the north hemisphere. See also the animation [129].

parameter [90] defined as $\phi_{\text{AH},\text{local}} := |\mathcal{B}^r / \sqrt{\rho_* v^r c}|$. They exhibit essentially the same time evolution, which indicates that the magnetically dominated region on the BH provides the Poynting flux in the magnetosphere.

Figure 3(b) plots the angular distribution of the Poynting luminosity per steradian evaluated on the sphere at

$r \approx 500$ km. It shows that the ring-shaped Poynting flux with $\approx 10^{49}$ erg/s/str exists along the BH spin axis with a collimation angle of $\lesssim 10^\circ$. The launching of the Poynting flux is in great contrast to the previously reported prompt collapse case [56]. We deduce that the discrepancy may be attributed to the shortness of their simulation of $t - t_{\text{merger}} \lesssim 0.1$ s and/or the different BNS model.

Figure 3(a) shows that for $t - t_{\text{merger}} \gtrsim 1$ s the isotropic-equivalent Poynting luminosity starts decreasing from 10^{49} erg/s. This is caused likely by the postmerger mass ejection [89,90]: the disk expands as the mass ejection proceeds, and the gas pressure around the funnel region decreases. The magnetic pressure in the magnetosphere remains because the magnetic flux does not significantly dissipate in the ideal magnetohydrodynamics. Since the collimated funnel structure of the magnetosphere is maintained by the balance of the magnetic pressure in the magnetosphere and the gas pressure from the disk, the opening angle of the magnetosphere increases. As the opening angle increases [130,131], the collimation of the magnetic flux becomes loosened, and the Poynting flux gradually decreases (see the animations [129,132]). We expect that in a few seconds, a substantial fraction of the disk matter will be ejected, and then, the magnetically driven Poynting flux will damp significantly.

Gravitational wave, neutrino, and kilonova—In addition to the Poynting flux-driven outflow, we also analyze the GW emission, neutrino emission, and ejection of neutron-rich matter in this simulation.

Figure 4(a) plots the gravitational waveform for the $l = m = 2$ mode characterized by the inspiral and subsequent quasinormal ringdown [133]. Figure 4(b) plots the neutrino luminosity for the electron, antielectron, heavy lepton, and total. The luminosity becomes maximum after the merger with $\approx 10^{53}$ erg/s. At $t - t_{\text{merger}} \approx 0.1$ s, the luminosity shows another peak since the MRI started to be fully resolved in the disk and the viscous heating driven by the MRI turbulent enhances the temperature (see Supplemental Material [120]). After this, the disk expansion and accretion onto the BH proceed, and the luminosity

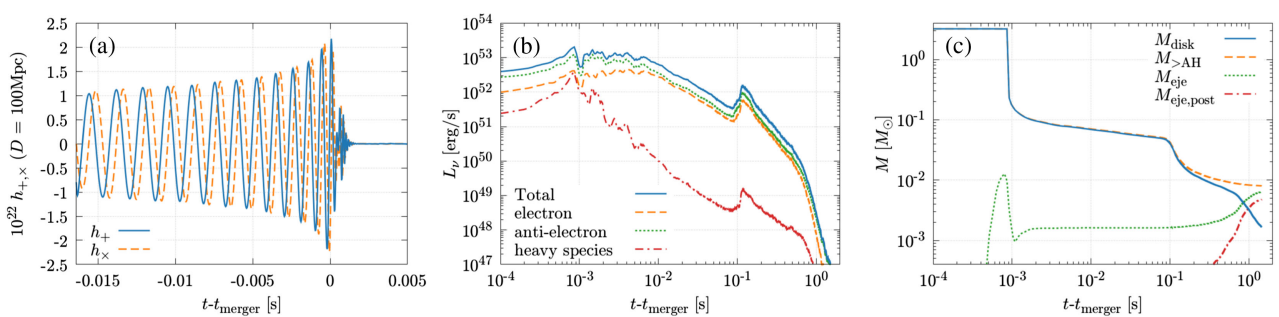


FIG. 4. The quantities related to multimessenger signals. Left: gravitational waveform for $l = m = 2$ mode. Middle: neutrino luminosity for the electron, antielectron, heavy lepton, and the total. Right: the baryonic mass of the matter remaining outside the apparent horizon (dashed), the disk (solid), the total ejecta (dotted), and the postmerger ejecta (dash-dotted).

decreases due to the temperature decrease because the neutrino energy emission rate is approximately proportional to T^6 [134]. As the neutrino luminosity steeply drops, the energy generated by the turbulent viscous heating can then be used for disk expansion and induces postmerger mass ejection [84,85,87,135–137]. Figure 4(c) plots the baryonic mass of the remnant, disk, total ejecta, and postmerger ejecta. During the merger stage, the dynamical ejecta with its mass $\approx 1.6 \times 10^{-3} M_\odot$ is launched. At $t - t_{\text{merger}} \approx 0.1$ s disk mass starts decreasing steeply due to the MRI-driven turbulent viscosity, and postmerger mass ejection sets in at $t - t_{\text{merger}} \approx 0.4$ s. At the end of the simulation, the disk mass decreases to $\approx 1.6 \times 10^{-3} M_\odot$ and the postmerger ejecta reaches $4.7 \times 10^{-3} M_\odot$, which is $\approx 8\%$ of the disk mass at $t - t_{\text{merger}} \approx 0.02$ s, making a total ejecta mass $6.3 \times 10^{-3} M_\odot$. This indicates that the kilonova light curve would be similar to that of the BNS merger leaving a short-lived hypermassive neutron star (HMNS) presented in Refs. [87,138] and is too faint to explain the observation of AT2017gfo.

Summary and discussion—We performed the first numerical-relativity simulation for prompt-collapse BNS merger which included neutrino radiation transfer and magnetohydrodynamics effects. The simulation lasts for ≈ 1.5 s after the merger, the longest among BNS merger simulations that self-consistently solve from the inspiral to the late postmerger stage. We focused on an asymmetric BNS merger so that the dynamical mass ejection and the massive disk formation proceed during the merger stage. We found that the gravitational waveforms, neutrino luminosity, and mass ejection are consistent with the previous simulations (e.g., Refs. [88,133]). Though it took ≈ 0.1 s after the merger until the MRI was fully resolved, it is unlikely to affect the postmerger mass ejection process, which takes ≈ 1 s.

We found that prompt-collapse BNS mergers can develop the magnetosphere which launches a collimated Poynting flux-driven outflow like the BNS merger that has a long-living HMNS as a remnant [114] or BHNS merger [89,90]. The MRI-driven $\alpha\Omega$ dynamo activity in the disk amplifies the magnetic field and provides an aligned magnetic field toward the polar region. Then, the BH spin further amplifies the magnetic field, generating a large-scale magnetic field due to the tower effect. It requires more than 0.1 s after the merger until the magnetosphere is developed and the isotropic-equivalent Poynting flux reaches as high as 10^{49} erg/s. We note that this timescale could be accelerated if the MRI is fully resolved right after the merger. At $t - t_{\text{merger}} \approx 1$ s the isotropic-equivalent luminosity of the collimated Poynting flux starts decreasing due to the increase of the opening angle of the magnetosphere, which is induced by the postmerger mass ejection. The conventional global MADness parameter [139] at the end of the simulation is ≈ 10 , and the system does not yet reach the MAD state. Therefore, we expect to have a

Poynting flux supply from the BH continued [70,140]. However, the magnetosphere will become further less collimated afterward, and the isotropic-equivalent luminosity evaluated at the opening angle of 10° is expected to keep decreasing (see also Supplemental Material [120]).

Our finding on a jet launching via the Blandford-Znajek mechanism aligns with many previous general relativistic magnetohydrodynamics simulations starting from an equilibrium disk around BH [70,73,139,141]. Those simulations showed that once the globally coherent magnetic field is provided from the disk to penetrate the BH, then the system launches the magnetically driven outflow. However, we argue that the origin and properties of such a globally coherent magnetic field were not well understood since the simulations mentioned above initialized magnetic fields by embedding the already globally coherent field. Further, assuming such a global magnetic field inside the merger remnant torus could result in an artificially strong relativistic outflow compared to the case in which the premerger magnetic field is initialized during the inspiral phase [48,88]. Reference [70] showed that the model with the purely toroidal magnetic field at the initial setup exhibits the magnetically driven outflow with its Poynting luminosity typically reaching $\sim 10^{48}$ erg/s about an order of magnitude higher than the current model. The BH properties and the disk mass resemble our current model, but the magnetic-field configuration right after the merger differs significantly in that the small-scale component is dominant in the large region (see also Supplemental Material [120]). We deduce the difference in Poynting luminosity from the magnetic field penetrating the BH, generated by the MRI-driven $\alpha\Omega$ dynamo from this small-scale magnetic field.

We have to note that in the present simulation, the maximum value of the initial magnetic-field strength is set to be 10^{15} G, which is as high as that for magnetars, i.e., much higher than observed in binary pulsars [26]. This treatment is motivated by an expectation that if the MRI is resolved well, the overall postmerger evolution processes remain essentially unchanged irrespective of the initial magnetic-field strength. However, in the simulation with an initially high magnetic field, not only the MRI but also the magnetic winding may play a role in enhancing the field strength in the remnant disk. The butterfly diagram of the averaged toroidal magnetic field shows that the aligned magnetic field at the polar region is generated not only by the periodic magnetic-field amplification due to the $\alpha\Omega$ dynamo but also by the winding of the magnetic field. We expect that in the system of a realistic magnetic-field strength, MRI-driven $\alpha\Omega$ dynamo activity will solely provide the magnetic field for magnetosphere formation. The higher-resolution simulation starting from a weaker premerger magnetic field should be conducted as future work.

Acknowledgments—We thank the members of the Computational Relativistic Astrophysics group in AEI

for useful discussions. We also thank Alexis Reboul-Salze for the helpful discussion. The numerical simulation of this work was performed on the computational resources of the supercomputer Fugaku provided by RIKEN through the HPCI System Research Project (Project IDs No. hp220174, No. hp220392, No. hp230084, No. hp230534, No. hp240039, No. hp240532, and No. hp250066). This work was supported by Grant-in-Aid for Scientific Research (No. 20H00158, No. 23H04900, No. 23H01172, and No. 23K25869) of JSPS/MEXT.

-
- [1] B. P. Abbott *et al.* (LIGO Scientific Collaboration and Virgo Collaboration), *Phys. Rev. Lett.* **119**, 161101 (2017).
 - [2] B. P. Abbott *et al.*, *Astrophys. J. Lett.* **848**, L12 (2017).
 - [3] B. P. Abbott *et al.*, *Astrophys. J.* **848**, L13 (2017).
 - [4] A. Goldstein *et al.*, *Astrophys. J. Lett.* **848**, L14 (2017).
 - [5] V. Savchenko *et al.*, *Astrophys. J. Lett.* **848**, L15 (2017).
 - [6] K. P. Mooley, A. T. Deller, O. Gottlieb, E. Nakar, G. Hallinan, S. Bourke, D. A. Frail, A. Horesh, A. Corsi, and K. Hotokezaka, *Nature (London)* **561**, 355 (2018).
 - [7] B. P. Abbott *et al.*, *Phys. Rev. Lett.* **121**, 161101 (2018).
 - [8] B. P. Abbott *et al.* (LIGO Scientific Collaboration and Virgo Collaboration), *Phys. Rev. X* **9**, 011001 (2019).
 - [9] S. De, D. Finstad, J. M. Lattimer, D. A. Brown, E. Berger, and C. M. Biwer, *Phys. Rev. Lett.* **121**, 091102 (2018); **121**, 259902(E) (2018).
 - [10] T. Narikawa, N. Uchikata, K. Kawaguchi, K. Kiuchi, K. Kyutoku, M. Shibata, and H. Tagoshi, *Phys. Rev. Res.* **2**, 043039 (2020).
 - [11] J. M. Lattimer and D. N. Schramm, *Astrophys. J. Lett.* **192**, L145 (1974).
 - [12] D. Eichler, M. Livio, T. Piran, and D. N. Schramm, *Nature (London)* **340**, 126 (1989).
 - [13] L.-X. Li and B. Paczyński, *Astrophys. J.* **507**, L59 (1998).
 - [14] B. D. Metzger, G. Martínez-Pinedo, S. Darbha, E. Quataert, A. Arcones, D. Kasen, R. Thomas, P. Nugent, I. V. Panov, and N. T. Zinner, *Mon. Not. R. Astron. Soc.* **406**, 2650 (2010).
 - [15] M. Tanaka and K. Hotokezaka, *Astrophys. J.* **775**, 113 (2013).
 - [16] S. Wanajo, Y. Sekiguchi, N. Nishimura, K. Kiuchi, K. Kyutoku, and M. Shibata, *Astrophys. J. Lett.* **789**, L39 (2014).
 - [17] Y. Utsumi *et al.* (J-GEM Collaboration), *Publ. Astron. Soc. Jpn.* **69**, 101 (2017).
 - [18] M. Tanaka *et al.*, *Publ. Astron. Soc. Jpn.* **69**, psx12 (2017).
 - [19] N. Domoto, M. Tanaka, S. Wanajo, and K. Kawaguchi, *Astrophys. J.* **913**, 26 (2021).
 - [20] N. Domoto, M. Tanaka, D. Kato, K. Kawaguchi, K. Hotokezaka, and S. Wanajo, *Astrophys. J.* **939**, 8 (2022).
 - [21] E. Nakar, *Phys. Rep.* **442**, 166 (2007), the Hans Bethe Centennial Volume 1906–2006.
 - [22] E. Berger, *Annu. Rev. Astron. Astrophys.* **52**, 43 (2014).
 - [23] B. P. Abbott *et al.*, *Astrophys. J. Lett.* **892**, L3 (2020).
 - [24] K. Kyutoku, S. Fujibayashi, K. Hayashi, K. Kawaguchi, K. Kiuchi, M. Shibata, and M. Tanaka, *Astrophys. J. Lett.* **890**, L4 (2020).
 - [25] M.-Z. Han, S.-P. Tang, Y.-M. Hu, Y.-J. Li, J.-L. Jiang, Z.-P. Jin, Y.-Z. Fan, and D.-M. Wei, *Astrophys. J. Lett.* **891**, L5 (2020).
 - [26] D. R. Lorimer, *Living Rev. Relativity* **11**, 8 (2008).
 - [27] N. Farrow, X.-J. Zhu, and E. Thrane, *Astrophys. J.* **876**, 18 (2019).
 - [28] M. Shibata, K. Taniguchi, and K. Uryū, *Phys. Rev. D* **71**, 084021 (2005).
 - [29] M. Shibata and K. Taniguchi, *Phys. Rev. D* **73**, 064027 (2006).
 - [30] K. Kiuchi, Y. Sekiguchi, M. Shibata, and K. Taniguchi, *Phys. Rev. D* **80**, 064037 (2009).
 - [31] K. Kiuchi, Y. Sekiguchi, M. Shibata, and K. Taniguchi, *Phys. Rev. Lett.* **104**, 141101 (2010).
 - [32] A. Bauswein, T. W. Baumgarte, and H. T. Janka, *Phys. Rev. Lett.* **111**, 131101 (2013).
 - [33] F. Zappa, S. Bernuzzi, D. Radice, A. Perego, and T. Dietrich, *Phys. Rev. Lett.* **120**, 111101 (2018).
 - [34] A. Bauswein, S. Blacker, V. Vijayan, N. Stergioulas, K. Chatzioannou, J. A. Clark, N.-U.F. Bastian, D. B. Blaschke, M. Cierniak, and T. Fischer, *Phys. Rev. Lett.* **125**, 141103 (2020).
 - [35] A. Bauswein, S. Blacker, G. Lioutas, T. Soulantasis, V. Vijayan, and N. Stergioulas, *Phys. Rev. D* **103**, 123004 (2021).
 - [36] R. Dudi, A. Adhikari, B. Brügmann, T. Dietrich, K. Hayashi, K. Kawaguchi, K. Kiuchi, K. Kyutoku, M. Shibata, and W. Tichy, *Phys. Rev. D* **106**, 084039 (2022).
 - [37] M. Shibata, K. Taniguchi, and K. Uryū, *Phys. Rev. D* **68**, 084020 (2003).
 - [38] R. Aguilera-Miret, D. Viganò, F. Carrasco, B. Miñano, and C. Palenzuela, *Phys. Rev. D* **102**, 103006 (2020).
 - [39] R. Aguilera-Miret, D. Viganò, and C. Palenzuela, *Astrophys. J. Lett.* **926**, L31 (2022).
 - [40] R. Aguilera-Miret, C. Palenzuela, F. Carrasco, and D. Viganò, *Phys. Rev. D* **108**, 103001 (2023).
 - [41] M. Anderson, E.W. Hirschmann, L. Lehner, S.L. Liebling, P.M. Motl, D. Neilsen, C. Palenzuela, and J.E. Tohline, *Phys. Rev. Lett.* **100**, 191101 (2008).
 - [42] K. Dionysopoulou, D. Alic, and L. Rezzolla, *Phys. Rev. D* **92**, 084064 (2015).
 - [43] B. Giacomazzo, L. Rezzolla, and L. Baiotti, *Mon. Not. R. Astron. Soc.* **399**, L164 (2009).
 - [44] B. Giacomazzo, L. Rezzolla, and L. Baiotti, *Phys. Rev. D* **83**, 044014 (2011).
 - [45] K. Kiuchi, K. Kyutoku, Y. Sekiguchi, M. Shibata, and T. Wada, *Phys. Rev. D* **90**, 041502(R) (2014).
 - [46] K. Kiuchi, P. Cerdá-Durán, K. Kyutoku, Y. Sekiguchi, and M. Shibata, *Phys. Rev. D* **92**, 124034 (2015).
 - [47] K. Kiuchi, K. Kyutoku, Y. Sekiguchi, and M. Shibata, *Phys. Rev. D* **97**, 124039 (2018).
 - [48] K. Kiuchi, L. E. Held, Y. Sekiguchi, and M. Shibata, *Phys. Rev. D* **106**, 124041 (2022).
 - [49] Y. T. Liu, S. L. Shapiro, Z. B. Etienne, and K. Taniguchi, *Phys. Rev. D* **78**, 024012 (2008).
 - [50] E. R. Most and E. Quataert, *Astrophys. J. Lett.* **947**, L15 (2023).
 - [51] E. R. Most, *Phys. Rev. D* **108**, 123012 (2023).
 - [52] P. Mösta, D. Radice, R. Haas, E. Schnetter, and S. Bernuzzi, *Astrophys. J. Lett.* **901**, L37 (2020).

- [53] C. Palenzuela, S. L. Liebling, D. Neilsen, L. Lehner, O. L. Caballero, E. O'Connor, and M. Anderson, *Phys. Rev. D* **92**, 044045 (2015).
- [54] C. Palenzuela, S. Liebling, and B. Miñano, *Phys. Rev. D* **105**, 103020 (2022).
- [55] C. Palenzuela, R. Aguilera-Miret, F. Carrasco, R. Ciolfi, J. V. Kalinani, W. Kastaun, B. Miñano, and D. Viganò, *Phys. Rev. D* **106**, 023013 (2022).
- [56] M. Ruiz and S. L. Shapiro, *Phys. Rev. D* **96**, 084063 (2017).
- [57] M. Ruiz, A. Tsokaros, V. Paschalidis, and S. L. Shapiro, *Phys. Rev. D* **99**, 084032 (2019).
- [58] M. Ruiz, A. Tsokaros, and S. L. Shapiro, *Phys. Rev. D* **101**, 064042 (2020).
- [59] M. Ruiz, A. Tsokaros, and S. L. Shapiro, *Phys. Rev. D* **104**, 124049 (2021).
- [60] L. Sun, M. Ruiz, S. L. Shapiro, and A. Tsokaros, *Phys. Rev. D* **105**, 104028 (2022).
- [61] Y. Sekiguchi, K. Kiuchi, K. Kyutoku, and M. Shibata, *Phys. Rev. Lett.* **107**, 051102 (2011).
- [62] Y. Sekiguchi, K. Kiuchi, K. Kyutoku, and M. Shibata, *Phys. Rev. D* **91**, 064059 (2015).
- [63] Y. Sekiguchi, K. Kiuchi, K. Kyutoku, M. Shibata, and K. Taniguchi, *Phys. Rev. D* **93**, 124046 (2016).
- [64] D. Radice, F. Galeazzi, J. Lippuner, L. F. Roberts, C. D. Ott, and L. Rezzolla, *Mon. Not. R. Astron. Soc.* **460**, 3255 (2016).
- [65] D. Radice, A. Perego, K. Hotokezaka, S. A. Fromm, S. Bernuzzi, and L. F. Roberts, *Astrophys. J.* **869**, 130 (2018).
- [66] F. Foucart, E. O'Connor, L. Roberts, L. E. Kidder, H. P. Pfeiffer, and M. A. Scheel, *Phys. Rev. D* **94**, 123016 (2016).
- [67] F. Foucart, M. D. Duez, R. Haas, L. E. Kidder, H. P. Pfeiffer, M. A. Scheel, and E. Spira-Savett, *Phys. Rev. D* **107**, 103055 (2023).
- [68] F. Zappa, S. Bernuzzi, D. Radice, and A. Perego, *Mon. Not. R. Astron. Soc.* **520**, 1481 (2023).
- [69] L. Lehner, S. L. Liebling, C. Palenzuela, O. L. Caballero, E. O'Connor, M. Anderson, and D. Neilsen, *Classical Quantum Gravity* **33**, 184002 (2016).
- [70] I. M. Christie, A. Lalakos, A. Tchekhovskoy, R. Fernández, F. Foucart, E. Quataert, and D. Kasen, *Mon. Not. R. Astron. Soc.* **490**, 4811 (2019).
- [71] M. D. Duez, Y. T. Liu, S. L. Shapiro, M. Shibata, and B. C. Stephens, *Phys. Rev. Lett.* **96**, 031101 (2006).
- [72] M. D. Duez, Y. T. Liu, S. L. Shapiro, M. Shibata, and B. C. Stephens, *Phys. Rev. D* **73**, 104015 (2006).
- [73] R. Fernández, A. Tchekhovskoy, E. Quataert, F. Foucart, and D. Kasen, *Mon. Not. R. Astron. Soc.* **482**, 3373 (2019).
- [74] K. Kiuchi, K. Kyutoku, and M. Shibata, *Phys. Rev. D* **86**, 064008 (2012).
- [75] L. Lehner, C. Palenzuela, S. L. Liebling, C. Thompson, and C. Hanna, *Phys. Rev. D* **86**, 104035 (2012).
- [76] M. Shibata, M. D. Duez, Y. T. Liu, S. L. Shapiro, and B. C. Stephens, *Phys. Rev. Lett.* **96**, 031102 (2006).
- [77] M. Shibata, Y. Suwa, K. Kiuchi, and K. Ioka, *Astrophys. J. Lett.* **734**, L36 (2011).
- [78] M. Shibata, S. Fujibayashi, and Y. Sekiguchi, *Phys. Rev. D* **103**, 043022 (2021).
- [79] M. Shibata, S. Fujibayashi, and Y. Sekiguchi, *Phys. Rev. D* **104**, 063026 (2021).
- [80] D. M. Siegel, R. Ciolfi, A. I. Harte, and L. Rezzolla, *Phys. Rev. D* **87**, 121302(R) (2013).
- [81] D. M. Siegel and B. D. Metzger, *Astrophys. J.* **858**, 52 (2018).
- [82] D. M. Siegel and B. D. Metzger, *Phys. Rev. Lett.* **119**, 231102 (2017).
- [83] B. C. Stephens, M. D. Duez, Y. T. Liu, S. L. Shapiro, and M. Shibata, *Classical Quantum Gravity* **24**, S207 (2007).
- [84] S. Fujibayashi, M. Shibata, S. Wanajo, K. Kiuchi, K. Kyutoku, and Y. Sekiguchi, *Phys. Rev. D* **101**, 083029 (2020).
- [85] S. Fujibayashi, M. Shibata, S. Wanajo, K. Kiuchi, K. Kyutoku, and Y. Sekiguchi, *Phys. Rev. D* **102**, 123014 (2020).
- [86] S. Fujibayashi, S. Wanajo, K. Kiuchi, K. Kyutoku, Y. Sekiguchi, and M. Shibata, *Astrophys. J.* **901**, 122 (2020).
- [87] S. Fujibayashi, K. Kiuchi, S. Wanajo, K. Kyutoku, Y. Sekiguchi, and M. Shibata, *Astrophys. J.* **942**, 39 (2023).
- [88] K. Kiuchi, S. Fujibayashi, K. Hayashi, K. Kyutoku, Y. Sekiguchi, and M. Shibata, *Phys. Rev. Lett.* **131**, 011401 (2023).
- [89] K. Hayashi, S. Fujibayashi, K. Kiuchi, K. Kyutoku, Y. Sekiguchi, and M. Shibata, *Phys. Rev. D* **106**, 023008 (2022).
- [90] K. Hayashi, K. Kiuchi, K. Kyutoku, Y. Sekiguchi, and M. Shibata, *Phys. Rev. D* **107**, 123001 (2023).
- [91] M. Shibata and T. Nakamura, *Phys. Rev. D* **52**, 5428 (1995).
- [92] T. W. Baumgarte and S. L. Shapiro, *Phys. Rev. D* **59**, 024007 (1998).
- [93] M. Campanelli, C. O. Lousto, P. Marronetti, and Y. Zlochower, *Phys. Rev. Lett.* **96**, 111101 (2006).
- [94] J. G. Baker, J. Centrella, D.-I. Choi, M. Koppitz, and J. van Meter, *Phys. Rev. Lett.* **96**, 111102 (2006).
- [95] P. Marronetti, W. Tichy, B. Brügmann, J. González, and U. Sperhake, *Phys. Rev. D* **77**, 064010 (2008).
- [96] D. Hilditch, S. Bernuzzi, M. Thierfelder, Z. Cao, W. Tichy, and B. Brügmann, *Phys. Rev. D* **88**, 084057 (2013).
- [97] K. Kyutoku, M. Shibata, and K. Taniguchi, *Phys. Rev. D* **90**, 064006 (2014).
- [98] K. Kawaguchi, K. Kyutoku, H. Nakano, H. Okawa, M. Shibata, and K. Taniguchi, *Phys. Rev. D* **92**, 024014 (2015).
- [99] A. Mignone, M. Ugliano, and G. Bodo, *Mon. Not. R. Astron. Soc.* **393**, 1141 (2009).
- [100] T. A. Gardiner and J. M. Stone, *J. Comput. Phys.* **227**, 4123 (2008).
- [101] D. S. Balsara, *J. Comput. Phys.* **228**, 5040 (2009).
- [102] A. Neuweiler, T. Dietrich, B. Brügmann, E. Giangrandi, K. Kiuchi, F. Schianchi, P. Mösta, S. Shankar, B. Giacomazzo, and M. Shibata, *Phys. Rev. D* **110**, 084046 (2024).
- [103] K. S. Thorne, *Mon. Not. R. Astron. Soc.* **194**, 439 (1981).
- [104] Y. Sekiguchi, *Prog. Theor. Phys.* **124**, 331 (2010).
- [105] Y. Sekiguchi, K. Kiuchi, K. Kyutoku, and M. Shibata, *Prog. Theor. Exp. Phys.* **2012**, 01A304 (2012).
- [106] A. W. Steiner, M. Hempel, and T. Fischer, *Astrophys. J.* **774**, 17 (2013).

- [107] F. X. Timmes and F. D. Swesty, *Astrophys. J.* **126**, 501 (2000).
- [108] LORENE, <http://www.lorene.obspm.fr/>.
- [109] A. Bauswein and N. Stergioulas, *Mon. Not. R. Astron. Soc.* **471**, 4956 (2017).
- [110] M. Shibata, S. Fujibayashi, K. Hotokezaka, K. Kiuchi, K. Kyutoku, Y. Sekiguchi, and M. Tanaka, *Phys. Rev. D* **96**, 123012 (2017).
- [111] Note that due to the lack of grid points resolving the BH, the BH spin gradually decreases numerically, so we switch to the Cowling approximation at $t - t_{\text{merger}} \approx 0.44$ s. This can be done safely since the baryonic mass of the disk is less than 1% of the BH mass at this time.
- [112] A. Brandenburg and K. Subramanian, *Phys. Rep.* **417**, 1 (2005).
- [113] A. Reboul-Salze, J. Guilet, R. Raynaud, and M. Bugli, *Astron. Astrophys.* **667**, A94 (2022).
- [114] K. Kiuchi, A. Reboul-Salze, M. Shibata, and Y. Sekiguchi, *Nat. Astron.* **8**, 298 (2024).
- [115] <https://www2.yukawa.kyoto-u.ac.jp/~kota.hayashi/SFHo125165-3D.mp4>
- [116] <https://www2.yukawa.kyoto-u.ac.jp/~kota.hayashi/SFHo125165-3Dvtkjs.html>
- [117] M. Shibata, Y. T. Liu, S. L. Shapiro, and B. C. Stephens, *Phys. Rev. D* **74**, 104026 (2006).
- [118] S. A. Balbus and J. F. Hawley, *Astrophys. J.* **376**, 214 (1991).
- [119] S. A. Balbus and J. F. Hawley, *Rev. Mod. Phys.* **70**, 1 (1998).
- [120] See Supplemental Material at <http://link.aps.org/supplemental/10.1103/PhysRevLett.134.211407>, which includes Refs. [121–125], for additional information on the dynamical mass ejection, the magnetic-field amplification, the disk properties right after the merger, the ejecta properties, and the magnetically dominated region.
- [121] S. Wanajo, S. Fujibayashi, K. Hayashi, K. Kiuchi, Y. Sekiguchi, and M. Shibata, *Phys. Rev. Lett.* **133**, 241201 (2024).
- [122] F. Foucart, M. D. Duez, L. E. Kidder, S. M. Nissanke, H. P. Pfeiffer, and M. A. Scheel, *Phys. Rev. D* **99**, 103025 (2019).
- [123] K. Hayashi, K. Kawaguchi, K. Kiuchi, K. Kyutoku, and M. Shibata, *Phys. Rev. D* **103**, 043007 (2021).
- [124] S. Chen, L. Wang, K. Hayashi, K. Kawaguchi, K. Kiuchi, and M. Shibata, *Phys. Rev. D* **110**, 063016 (2024).
- [125] K. Kawaguchi, N. Domoto, S. Fujibayashi, H. Hamidani, K. Hayashi, M. Shibata, M. Tanaka, and S. Wanajo, *Mon. Not. R. Astron. Soc.* **535**, 3711 (2024).
- [126] <https://www2.yukawa.kyoto-u.ac.jp/~kota.hayashi/SFHo125165-2Drt.mp4>
- [127] A. Reboul-Salze *et al.* (to be published).
- [128] R. D. Blandford and R. L. Znajek, *Mon. Not. R. Astron. Soc.* **179**, 433 (1977).
- [129] <https://www2.yukawa.kyoto-u.ac.jp/~kota.hayashi/SFHo125165-pf.mp4>
- [130] M. Pais, T. Piran, Y. Lyubarsky, K. Kiuchi, and M. Shibata, *Astrophys. J. Lett.* **946**, L9 (2023).
- [131] M. Pais, T. Piran, K. Kiuchi, and M. Shibata, *Astrophys. J.* **976**, 35 (2024).
- [132] <https://www2.yukawa.kyoto-u.ac.jp/~kota.hayashi/SFHo125165-2Dxz.mp4>
- [133] K. Hotokezaka, K. Kiuchi, K. Kyutoku, H. Okawa, Y.-i. Sekiguchi, M. Shibata, and K. Taniguchi, *Phys. Rev. D* **87**, 024001 (2013).
- [134] G. M. Fuller, W. A. Fowler, and M. J. Newman, *Astrophys. J.* **293**, 1 (1985).
- [135] R. Fernández and B. D. Metzger, *Mon. Not. R. Astron. Soc.* **435**, 502 (2013).
- [136] O. Just, A. Bauswein, R. A. Pulpillo, S. Goriely, and H.-T. Janka, *Mon. Not. R. Astron. Soc.* **448**, 541 (2015).
- [137] O. Just, S. Goriely, H. T. Janka, S. Nagataki, and A. Bauswein, *Mon. Not. R. Astron. Soc.* **509**, 1377 (2022).
- [138] K. Kawaguchi, S. Fujibayashi, N. Domoto, K. Kiuchi, M. Shibata, and S. Wanajo, *Mon. Not. R. Astron. Soc.* **525**, 3384 (2023).
- [139] A. Tchekhovskoy, R. Narayan, and J. C. McKinney, *Mon. Not. R. Astron. Soc.* **418**, L79 (2011).
- [140] O. Gottlieb *et al.*, *Astrophys. J. Lett.* **954**, L21 (2023).
- [141] M. Liska, A. Tchekhovskoy, and E. Quataert, *Mon. Not. R. Astron. Soc.* **494**, 3656 (2020).